SUPPLEMENTAL MATERIALS for Ragusa et al.

Supplemental Figures

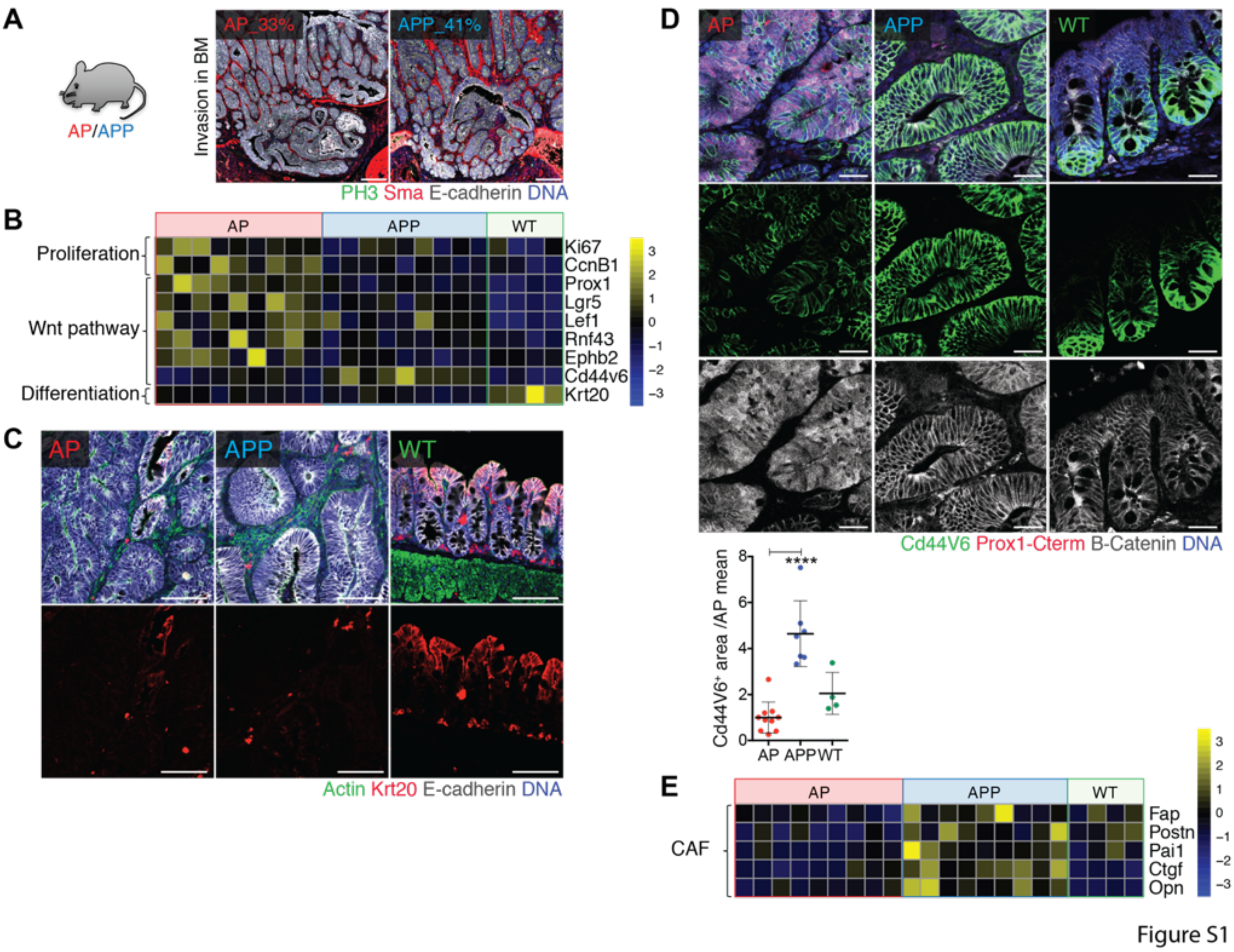

Supplemental Figure 1, related to Figure 2. Further characterization of APP and AP genetic models. (**A**) Examples of invasive AP and APP tumors breaching the basement membrane. Staining for phosphohistone H3 (PH3, green), α-Sma (red), E-cadherin (white) and DNA (blue). Scale bar, 200µm. Tumors resected one month after induction. The percentage of invasive tumors is indicated for each genotype, n=16. (**B**) Heatmap of WNT target genes, proliferation and differentiation markers in AP and APP tumors, n=9, or normal caecum, n=4. Relative to RT-qPCR. (**C**) Representative staining for Cd44v6 (green), PROX1 (red), ß-catenin (white) and DNA (blue) in AP (n=10) or APP (n=7) tumors and wild type intestine, n=4. Nuclear and cytoplasmic ß-catenin identify cells with high Wnt signaling. Scale bar, 25µm. Data were analysed with one-way ANOVA with Tukey's multiple comparison test (****p ≤0.0001), and shown as scatter dot plot ±SD. Each dot represents a single mouse. (**D**) Absence of differentiation in AP and APP tumors. Staining for KRT20 (differentiation marker, red), E-cadherin (epithelial cells, white), total actin (for stromal and epithelial cells recognition, green) and DNA (blue). Scale bar, 50µm. (**E**) Increased expression of cancer-associated fibroblast markers in APP tumors. Heatmap of the indicated gene. AP or APP, n=9; normal caecum, n=4.

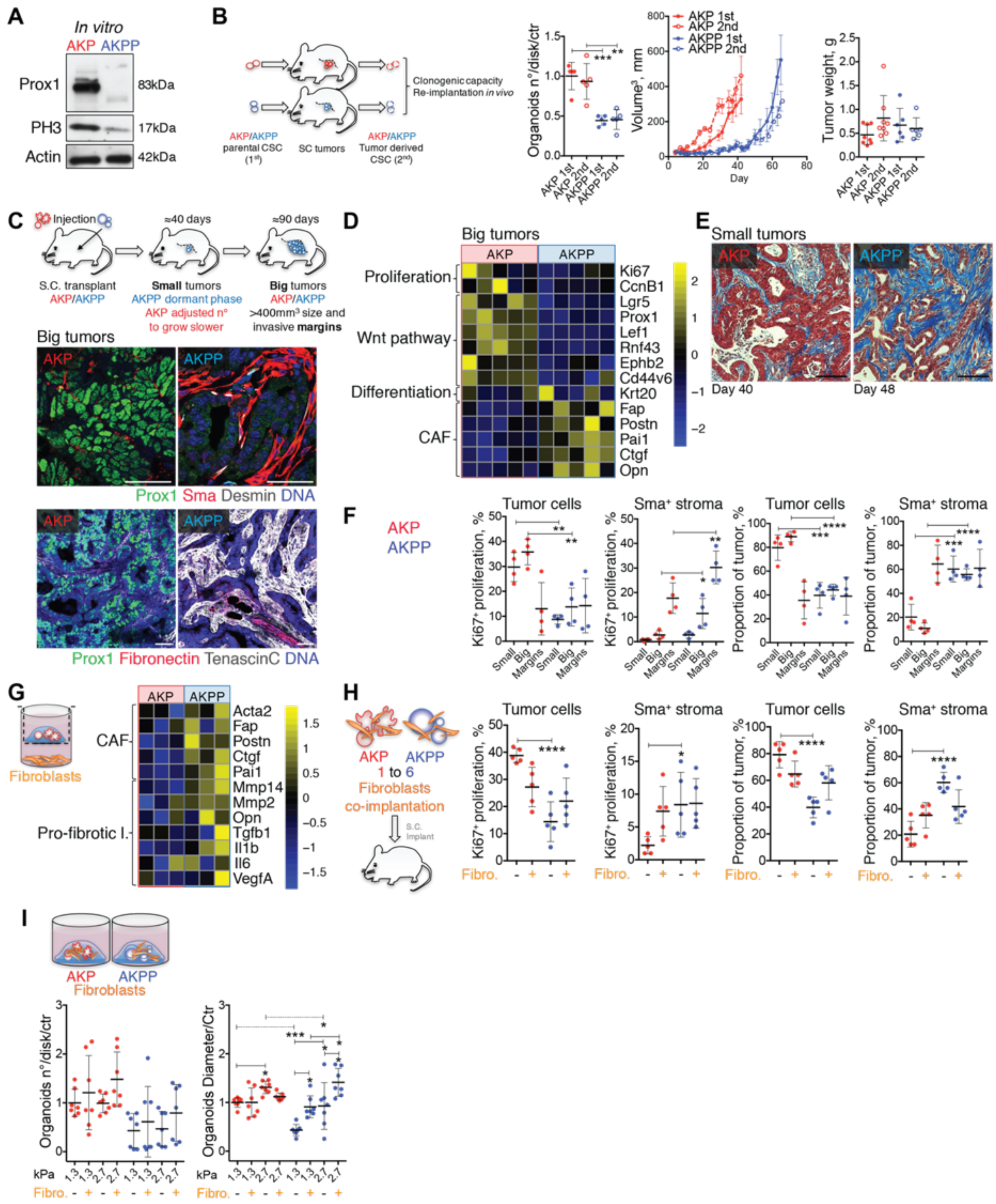

Supplemental Figure 2, related to Figure 3. Mutually beneficial interactions between *Prox1*-deficient tumor cells and fibroblasts. (**A**) Proliferation of AKP and AKPP organoids. Western blot for PROX1, phosphohistone H3 (proliferation) and ß-actin (normalization). (**B**) Comparable *in vitro* and *in vivo* growth of parental and tumor-derived AKP and AKPP organoids. AKP and AKPP parental organoids (1^{st}) were injected in NSG mice and new organoids harvested from large tumors (2^{nd}) were re-grown *in vitro* (n=5 each) or re-implanted *in vivo.* 50 AKP or 300 AKPP were implanted per mouse, AKP (n=8), AKPP (n=6). *In vitro* data are presented as fold change over AKP 1^{st} mean. (**C**) Desmoplasia in advanced tumors. Tumors were resected at day 26 (AKP) or 93 (AKPP). Upper row: PROX1 (green), α-Sma (red), Desmin (white) and DNA (blue); lower row: PROX1 (green), fibronectin (red), tenascin C (white) and DNA (blue). Scale bars, 50μm. **(D)** Heatmap of proliferation, Wnt signaling, differentiation and CAF markers in advanced AKP and AKPP tumors. Each column represents an individual tumor (n=5). (**E**) Increased stroma in small, apparently dormant AKPP tumors. Tumors were resected when they become palpable at day 40 (AKP) or 48 (AKPP). Masson's trichrome staining. Scale bar, 50µm. (**F**) Quantification of PROX1 levels, α-Sma^+ stromal content and $Ki67^+$ proliferation in small and advanced AKP and AKPP tumors. Data are presented as percentage of total population (n=4). (**G**) Heatmap of CAF activation markers and pro-fibrotic ligands in AKP or AKPP co-cultured fibroblasts (n=3). (**H**) Quantification of PROX1 expression, α-Sma^+ stromal content and proliferation in AKP and AKPP tumors co-implanted with intestinal fibroblasts. Related to figure 3K. Data analysis as for figure F (n=5). (**I**) Quantifications of the number and the average diameters of individual AKP or AKPP organoids cultured in the presence of fibroblasts, in synthetic hydrogels, at the indicated starting stiffness conditions. Data are presented as fold change over AKP 1.3kPa control (n=7). All data were analysed with one-way (scatter plots) or two-way (growth curves) ANOVA with Tukey's multiple comparison, and shown mean±SD. *p ≤0.05; **p ≤0.01; ***p ≤0.001; ****p ≤0.001. Each dot represents individual mouse or *in vitro* repeat from merged experiments.

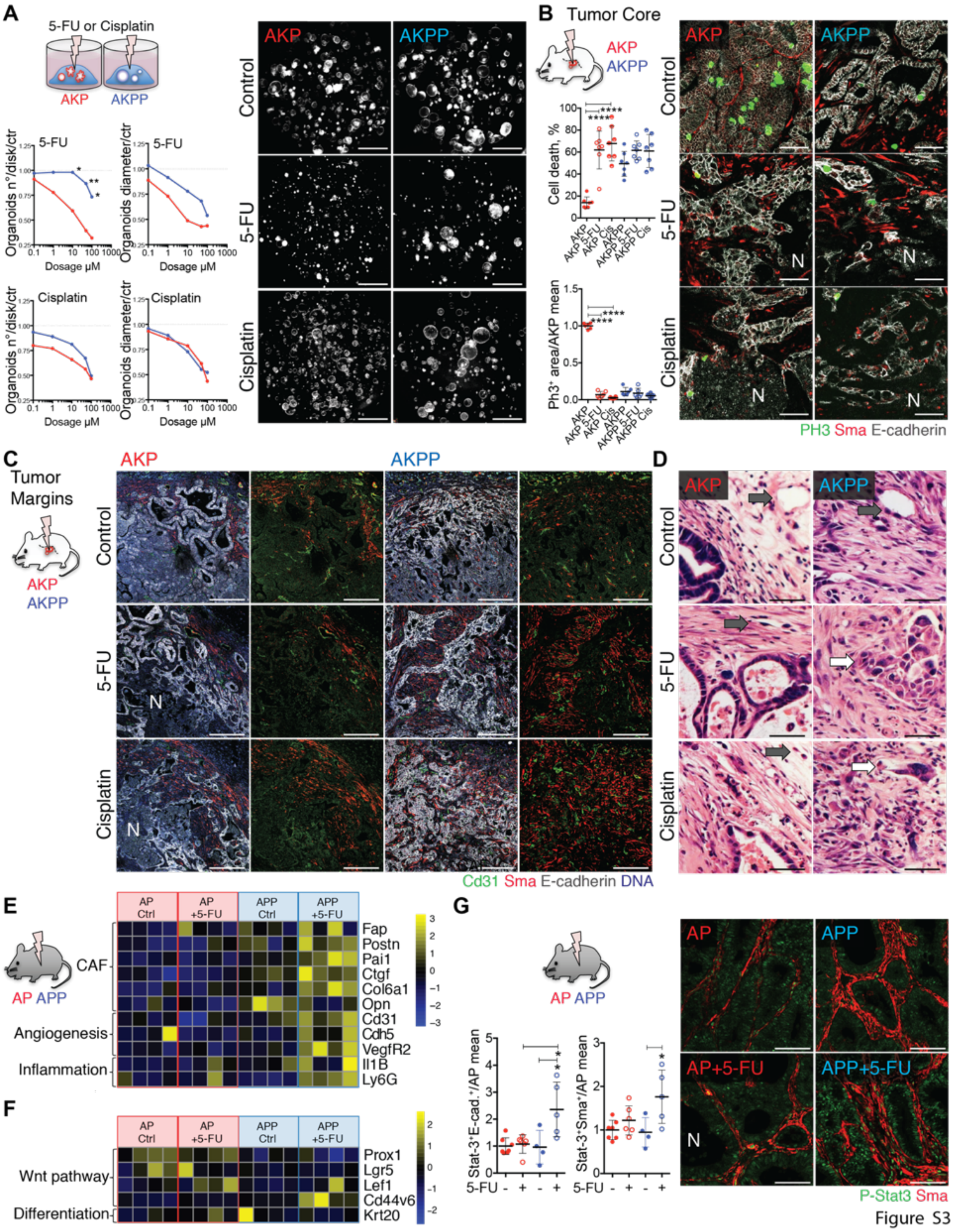

Supplemental Figure 3, related to Figure 4. Chemotherapy increases invasion and survival of *Prox1*-deficient tumor cells *in vivo*. (**A**) Growth curves and bright field view of AKP or AKPP organoids after treatment with 0.1, 1, 10, 50 or 100μM of 5-FU or cisplatin, total number of organoids per well and average organoid diameter were quantified, n=1. Scale bar, 1.2mm. (**B**) Necrotic AKP and AKPP core tumor areas after treatment with 5-FU or cisplatin and related quantification. Staining for phosphohistone H3 (green), α-Sma (red) and E-cadherin (white). N, necrotic tumor glands. Scale bar, 50μm. Quantification of cell death or PH3^{+} proliferating cells, in equivalent tumor areas (n=7). Cell death shown as percentage of necrotic tumor glands, proliferation as fold change over the AKP control mean. (**C**) Low magnification view of chemotherapy effect on AKP and AKPP tumor margins. Staining for CD31 (green), α-Sma (red), E-cadherin (white) and DNA (blue). N, necrotic areas. Scale bar, 100µm. (**D**) Examples of intravascular invasion in chemotherapy-treated AKP tumor margins. H&E staining. Grey arrows, metastasis-free peritumoral vessel; white arrows, intravascular invasion. Scale bar, 25µm. (**E**) 5-FU effect on desmoplasia and inflammation. Heatmap of CAF, angiogenic and inflammation markers in AP and APP tumors (n=4). (**F**) 5-FU does not affect WNT signaling. Heatmap of WNT targets and differentiation marker Krt20 in AP and APP tumors. (**G**) 5-FU increases the accumulation of phosphorylated Stat3 in APP tumors. Staining for phospho-STAT3 (green) and α-Sma (red), and related quantification. N, necrotic tumor glands. Scale bar, 50µm. Quantification for phospho-STAT3 levels in cancer cells (P-STAT3^{+}/E-cadherin^{+}) and fibroblasts (P-STAT3^{+}/α-Sma^{+}) in AP and APP tumors. Data are presented as fold change over the AP untreated mean. One-way (scatter plots) or two-way (dose response curves) ANOVA with Tukey's multiple comparison. Scatter plot data are shown as mean±SD. *p ≤0.05; **p ≤0.01; ****p ≤0.001. Each dot represents an individual mouse.

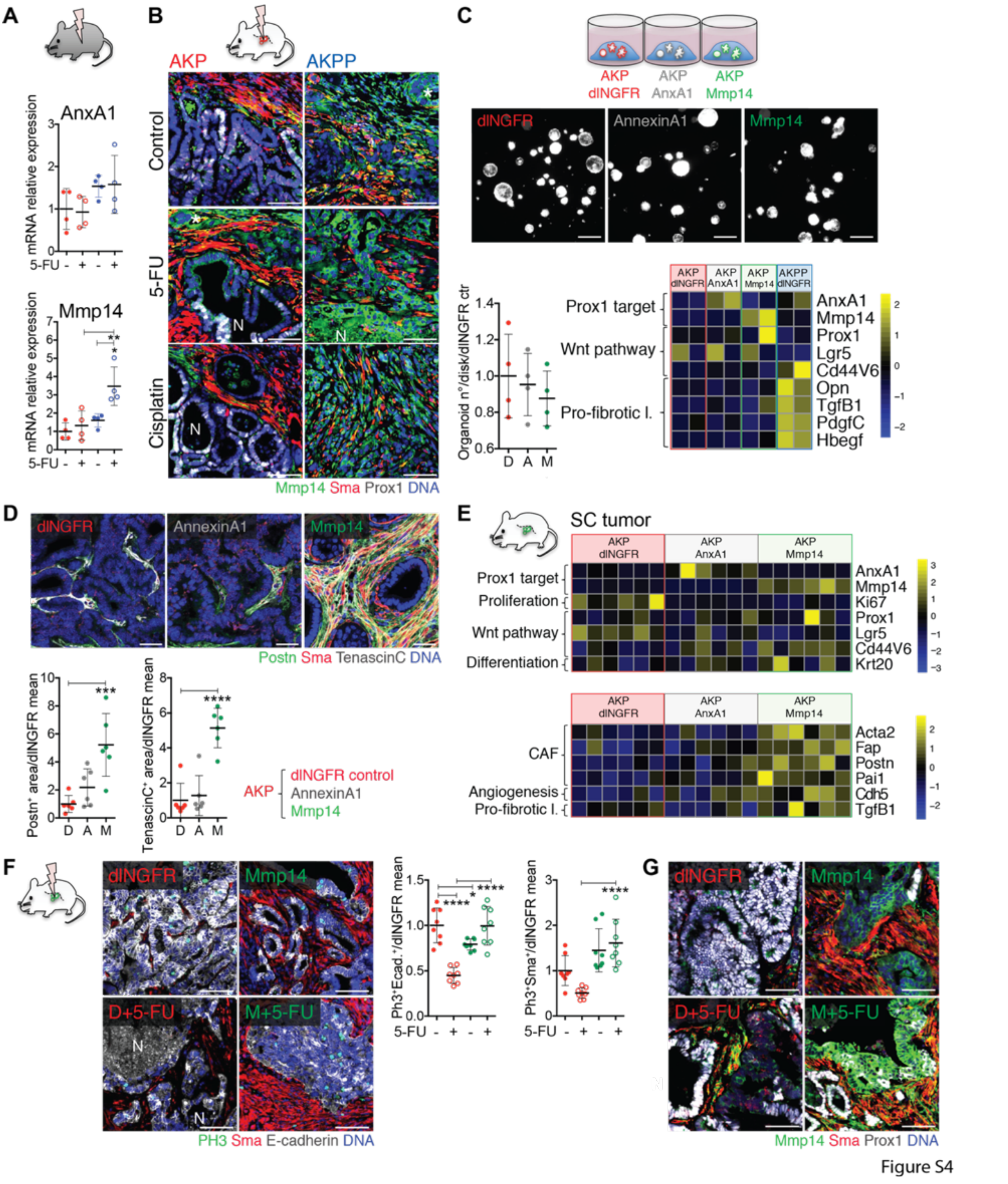

Figure S4

Supplemental Figure 4: related to Figure 5. MMP14 overexpression is sufficient to generate highly desmoplastic tumors. (**A**) 5-FU effect on MMP14 and ANXA1 expression in *Prox1*-deficient tumors. RT-qPCR data are presented as fold change over AP untreated means. (**B**) Staining for MMP14 (green), α-Sma (red), PROX1 (white) and DNA (blue). N, necrotic tumor glands. Scale bar, 50µm. (**C**) *Anxa1* and *Mmp14* overexpression in organoids. Bright field view, clonogenic capacity of AKP control dlNGFR «D», ANXA1 «A» and MMP14 «M» producing organoids (n=4), and heatmap for the indicated genes (n=2). Data are presented as fold change over the AKP control mean. Scale bar, 1.2mm. (**D**) Stromal expansion in MMP14-AKP tumors. Representative pictures and related quantification. Staining for periostin (fibroblasts, green), α-Sma (fibroblasts, red), tenascin C (ECM, white) and DNA (blue). Data are presented as fold change over the AKP control mean. Scale bar, 50µm. (**E**) *Mmp14* and *Anxa1* overexpression in tumors. Effect on WNT pathway, CAF, angiogenic and pro-fibrotic markers. Heatmaps of the indicated genes, n=6. (**F**) 5-FU does not blunt proliferation in MMP14-AKP tumors. Staining of control and treated dlNGFR- and MMP14-AKP tumors, for phosphohistone H3 (proliferation, green), α-Sma (fibroblasts, red), E-cadherin (tumor cells, white) and DNA (blue). N, necrotic tumor glands. Scale bar, 50µm. $PH3^+E\text{-cadherin}^+$ and $PH3^+\alpha\text{-Sma}^+$ proliferating tumor cells or fibroblasts. Data are presented as fold change over the dlNGFR untreated mean. (**G**) 5-FU enhances MMP14 expression by CAFs in MMP14-AKP tumors, related to figure 5H. Staining for MMP14 (green), α-Sma (fibroblasts, red), PROX1 (white) and DNA (blue). N, necrotic tumor glands. Scale bar, 50µm. One-way ANOVA with Tukey's multiple comparison, and presented as scatter plot with mean±SD. *p ≤0.05; **p ≤0.01; ***p ≤0.001; **** p ≤0.0001.

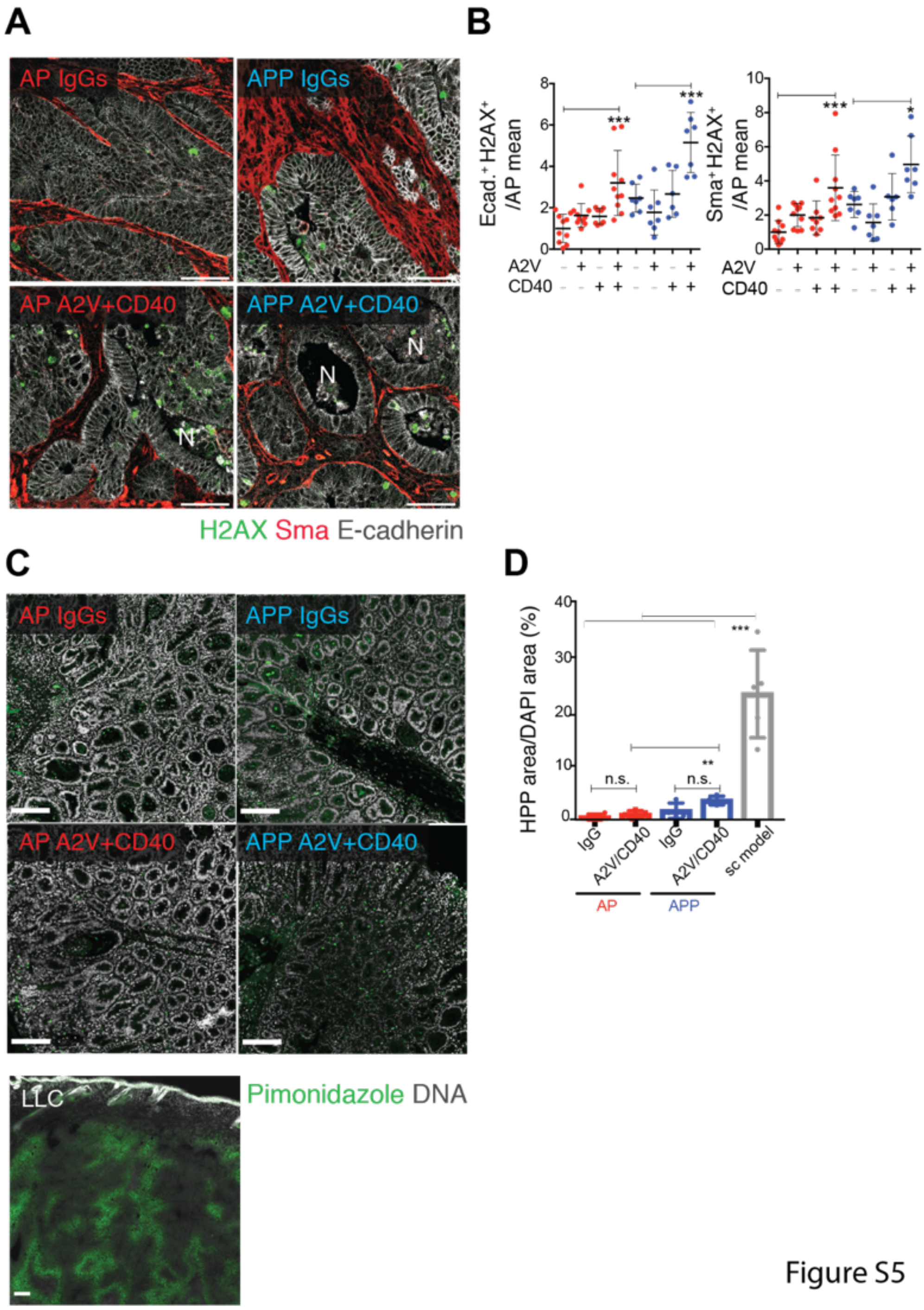

Supplemental Figure 5, related to Figure 6. Characterization of cell death and hypoxia in AP and APP tumors. (**A**) DNA damage in tumors treated with A2V+aCD40. Staining for γH2AX (green), α-Sma (red) and E-cadherin (white). N, necrotic tumor glands. Scale bar, 50µm. (**B**) Quantification of γH2AX accumulation in cancer and stromal cells. Proportions of $\gamma H2AX^+$E-cadherin$^+$ and $\gamma H2AX^+\alpha$-Sma$^+$ areas of total E-cadherin$^+$ and α-Sma$^+$ areas, presented as fold change over the AP IgGs mean. (**C**) Representative images of hypoxia in AP and APP tumors treated with control IgG and A2V+aCD40 and of subcutaneous Lewis lung cell carcinoma (LLC) tumors. Staining for pimonidazole adducts (green) and DNA (white). Scale bar, 200 µm. (**D**) Quantification of hypoxia from C. Percentage of hypoxic area normalized to total tumor area.

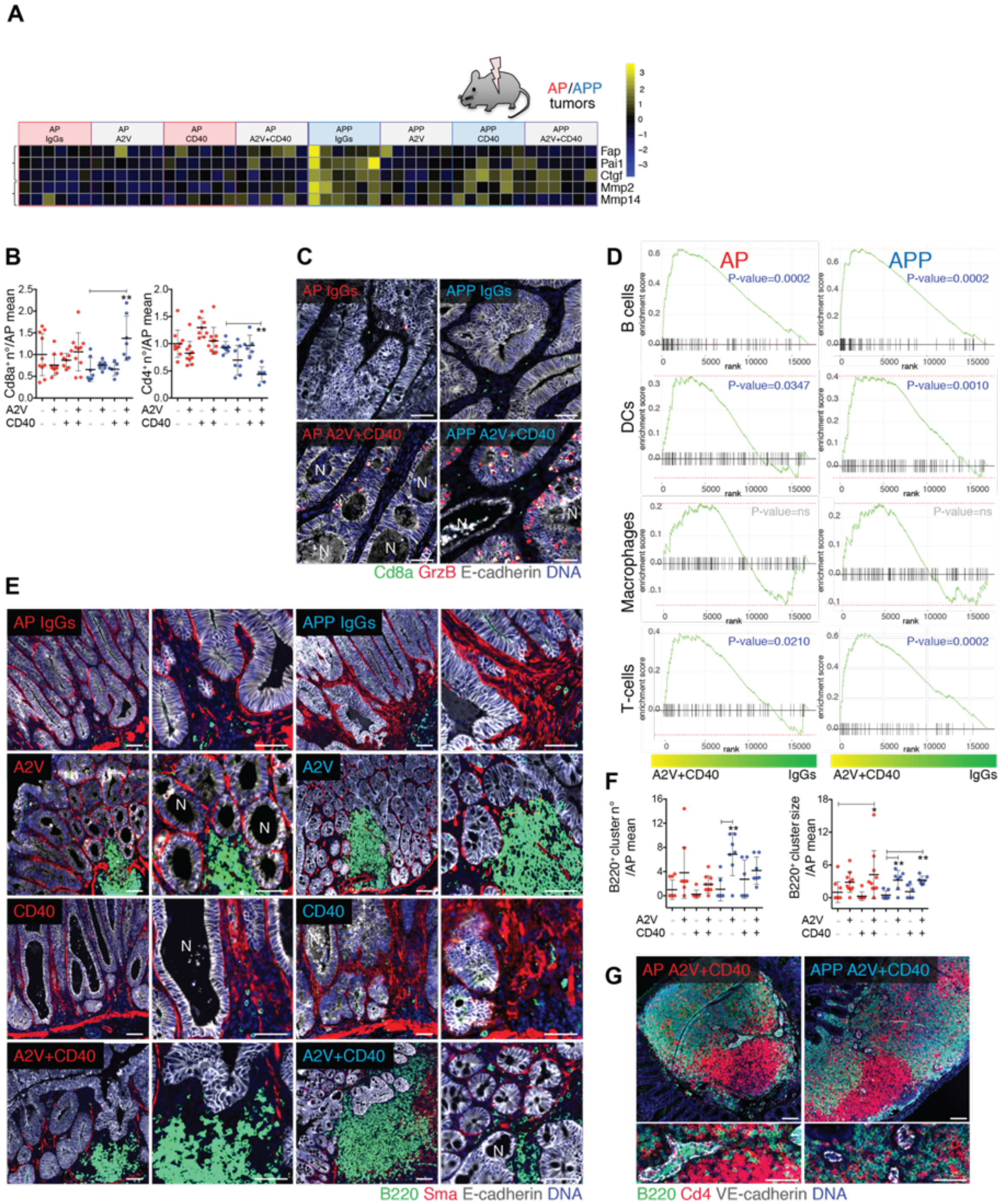

Figure S6

Supplemental Figure 6, related to Figure 6. Characterization of immune infiltrates in AP and APP tumors. (**A**). Heatmap of CAF markers and matrix metalloproteases in APP tumors treated with A2V and A2V+aCD40, n=6. (**B**) Quantification for intratumoral CD8^{+} and CD4^{+} T cells in AP and APP tumors under the indicated treatments, related to figure 6I. Total CD8a^{+} or CD4^{+} cells numbers in equal tumor areas, as fold change over the AP IgGs mean. (**C**) Representative intratumoral CTLs in AP and APP tumors, related to figure 6J. Staining for CD8a (green), granzyme B (cytotoxic marker, red), E-cadherin (tumor cells, white) and DNA (blue). N, necrotic tumor glands. Scale bar, 50µm. (**D**) Enrichment for B, T cell and DC, but not macrophage signatures in AP (n=4) or APP (n=3) tumors treated with A2V+aCD40 *vs*. respective control tumors (n=6 per genotype). Cell type-specific signatures were obtained from (*53*) and enrichment analysis was performed using GSEA. (**E**) A2V and A2V+aCD40 promote the formation of B cells clusters. Staining for B220 (B-cells, green), α-Sma (fibroblasts, red), E-cadherin (tumor cells, white) and DNA (blue). N, necrotic tumor glands. Scale bar, 50µm. (**F**) Quantification for $B220^+$ clusters number or size in control or treated AP and APP tumors, as fold change over the AP IgGs mean. (**G**). Compartmentalization of T and B cells and HEV-like vessels in $B220^+$ clusters in AP and APP treated tumors. Staining for B220 (B cells, green), CD4 (red), VE-cadherin (ECs, white) and DNA (blue). Lower row: high magnification view of HEV-like vessels. Scale bar, 100µm (upper row), 50µm (lower row). Data were analyzed with one-way ANOVA with Tukey's multiple comparison, and presented as scatter plot with mean±SD. *p ≤0.05; **p ≤0.01; ***p ≤0.001.

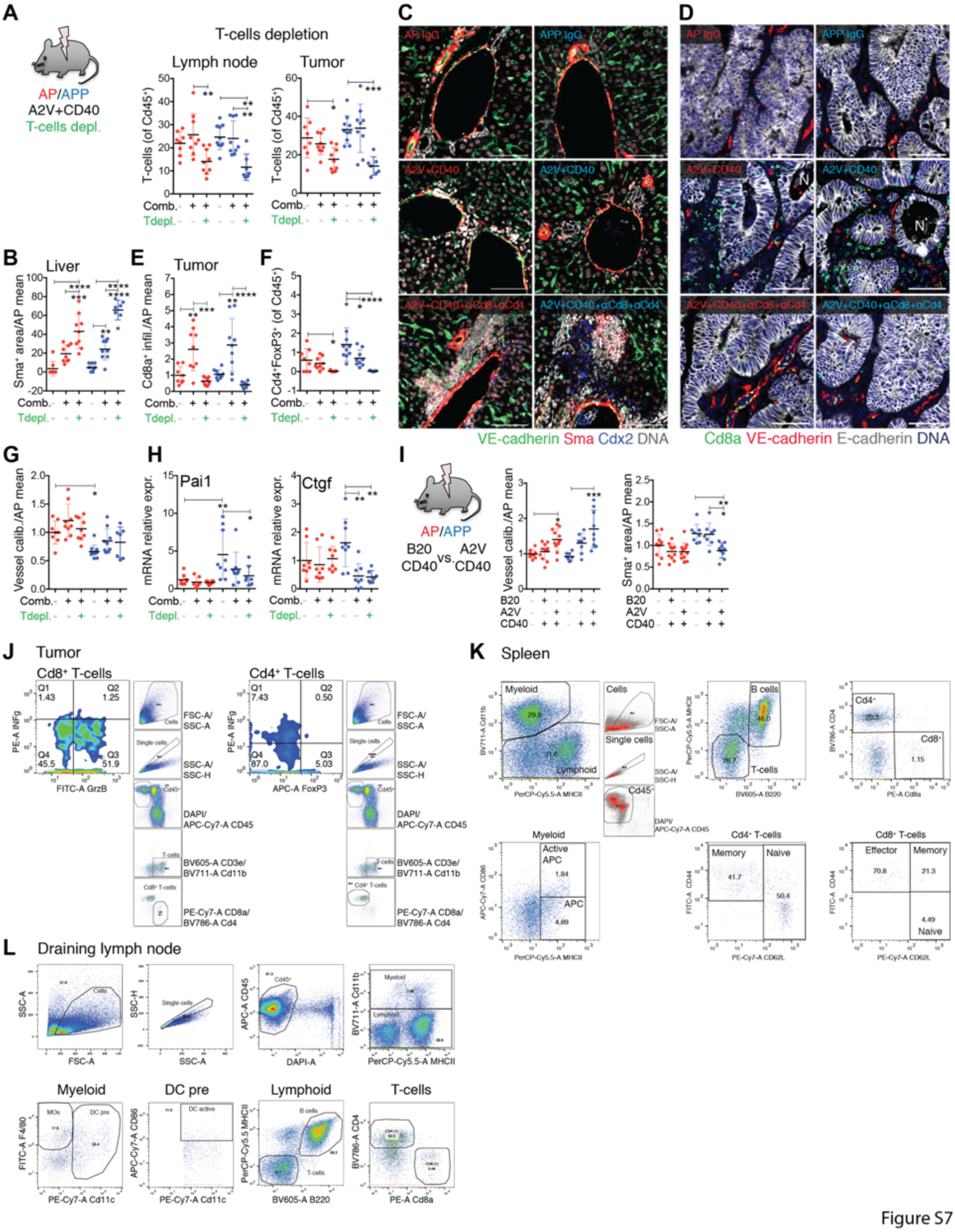

Supplemental Figure 7, Related to Figure 7. Further characterization of A2V+aCD40 and B20+aCD40 effects. (**A**) T cells depletion in A2V+aCD40 treated AP and APP models. FACS analysis confirmation of lymph node (CD11b^{neg}B220^{neg}MHCII^{neg}) and tumor (CD11b^{neg}CD3^{+}) T cells depletion. Data are expressed as percentage of total CD45^{+} cells. (**B**) A2V+aCD40 treatment induces liver fibrosis after T cells depletion. Quantification for α-Sma^{+} area per corresponding liver field. Data are presented as fold change over the AP IgGs mean. (**C**) Representative stainings of mouse livers for VE-cadherin (ECs green), α-Sma (fibroblasts, red), CDX2 (tumor cells, blue) and DNA (white). Scale bar, 50µm. (**D**) Representative confirmation of tumor $CD8^+$ T cell depletion. Staining for CD8a (green), VE-cadherin (ECs, red) and E-cadherin (tumor cells, white) and DNA (blue). N, necrotic tumor glands. Scale bar, 50µm. (**E**) Intraepithelial $CD8^+$ T cells infiltration. Quantification for the average number of $CD8a^+$ T cells infiltrated in the tumor glands, in equal areas, as fold change over AP IgGs mean. (**F**) FACS analysis of T-regs accumulation ($CD11b^{neg}CD3^+CD4^+Ifn\gamma^{neg}FoxP3^+$) in A2V+aCD40 treated tumors. Data are expressed as percentage of total $CD45^+$ cells. (**G**) Effect on tumor angiogenesis. VE-cadherin$^+$ individual vessel size, in equivalent tumor areas. Data are presented as fold change over the AP IgGs mean. (**H**) Tumor stromal activation markers levels. RT-qPCR analysis for TGFß targets *Pai1* and *Ctgf* in total tumor lysates, as fold change over the AP IgGs mean. (**I**) Comparison of A2V+aCD40 *vs*. B20+aCD40 effects on tumor angiogenesis and stroma ablation. VE-cadherin$^+$ individual vessel size, or α-Sma$^+$ stromal area, per equivalent fields. Data are presented as fold change over the AP IgGs mean. One-way ANOVA with Tukey's multiple comparison, and presented as scatter plot with mean±SD. *p ≤0.05; **p ≤0.01; ***p ≤0.001; ****p ≤0.0001. J to L: FACS analysis gating strategy used respectively for (**J**) tumor; (**K**) draining mesentheric lymph node; or (**L**) spleen.

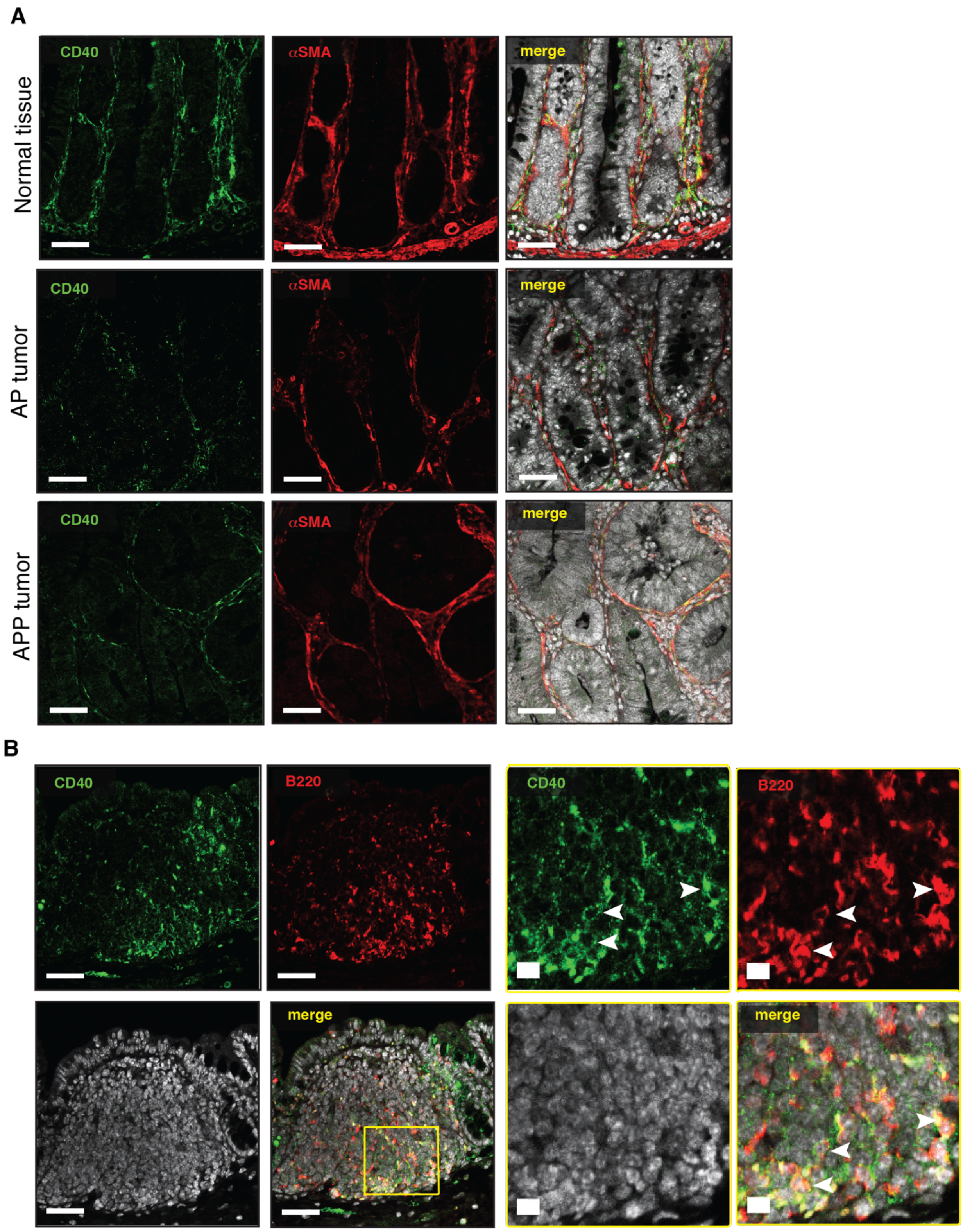

Supplemental Figure 8, related to Discussion. CD40 is expressed in normal intestinal and cancer-associated fibroblasts. (**A**) CD40 is expressed by a subset of α-Sma$^+$ normal intestinal fibroblasts and cancer-associated fibroblasts of AP and APP tumors. Staining for CD40 (green), α-Sma (red) and DNA (white). Scale bar, 100μm. (**B**) CD40 is expressed by B cells in tumor-associated lymphoid structures in APP tumors. Staining for CD40 (green), B220 (red) and DNA (white). Scale bar, 100μm.

Supplemental Methods

Human Studies

114 MMR^+ human tumors were stained for PROX1(R&D) as previously described (1). Tumors were scored for the PROX1 tumor cells nuclear expression, and for the stromal cells abundance over the total tumor area. PROX1 score 1 indicate PROX1 markedly expressed in less than 25% of the epithelial tumor cells; 2, PROX1 expression in between 25 and 50%; 3 in between 50 and 75%; 4 if PROX1 expression was high in more than 75% of tumor cells. Stromal score is related to the abundance of non-epithelial tumor cells present in the total tumor population. Score 1 indicates stromal percentage of less than 25% out of total tumor area, 2 stroma between 25 and 50%, 3 between 50 and 75%, and 4 for more than 75% stroma. Patients details are listed in Supplemental Table 1.

Animal Studies

$Apc^{fl/fl}$;$Kras$-$^{LSL\text{-}G12D}$;$Tp53^{fl/f}$; *villin*-Cre^{ERT2} (AKP) and $Apc^{fl/fl}$; $Tp53^{fl/f}$; *villin*-Cre^{ERT2} mice (AP) have been described previously (1-4). The $Apc^{fl/fl}$; $Tp53^{fl/f}$;$Prox1^{fl/fl}$;*villin*-Cre^{ERT2} (APP) mice were generated by crossing AP mice with $Prox1^{fl/fl}$ mice (5-9). 9-12 week old male and female littermates (mixed C57BL/6/SV129) were randomized into matched cohorts, based on sex and age. AP and APP orthotopic tumors were induced by intracaecal injection of 15µl of 10mg/ml tamoxifen (Sigma), dissolved in Cremophor EL (Sigma) using an Omnican 50 syringe with 28G needle (Braun) under a stereomicroscope as described previously (10). In chemotherapy experiments, 2.5 weeks after tumor induction mice were injected i.p. with 10mg/kg 5-FU or PBS twice a week for 1.5 weeks. For A2V+aCD40 treatment, two weeks after tumor induction, mice were injected i.p. with: 20mg/kg of anti-mouse A2V (muIgG2a, Roche) or MOPC-21 IgG2 control once a week; and 10mg/kg anti-mouse CD40 (FGK4.5 muIgG1, Roche) or MOPC-21 IgG1 control once. For comparison between A2V+aCD40 and B20+aCD40, mice were injected i.p. with 10mg/kg of anti-mouse B20 (B20.4.1, Roche). For T cells depletion, mice were injected with 10mg/kg i.p, twice a week with anti-mCD4 (clone GK1.5, BioXcell) and anti-mCD8a (clone 2.43, BioXcell), or 20mg/Kg of control rat IgG2b (clone LTF-2, BioXcell). T cell depletion experiment treatments lasted 9 days because of high morbidity in T cell depletion/A2V+aCD40 group. For hypoxia analyses, mice were injected with 60 mg/kg of pimonidazole (Hypoxyprobe, HPI) 30 min prior to sacrifice.

For subcutaneous tumor experiments, organoids were injected in the flank of 8-12 weeks-old NOD-Scid; IL-2R$\gamma^{-/-}$ mice using a 20G needle (Braun). Tumor width (W) and length (L) were measured with calipers and the volume was calculated as $\pi/6 x L x (W^2)$. For comparison of AKP vs AKPP responses to chemotherapy, treatment was started when all tumors reached at least 130 mm^3. 10mg/kg 5-FU (Sigma) in PBS, 3mg/kg cisplatin (Millipore) in PBS with ultra-sonication prior to injection or PBS were injected i.p. twice a week. In dlNGFR-AKP and MMP14-AKP experiments mice were treated when all tumors reached minimum 100mm^3 with 10mg/kg 5-FU or PBS (Sigma) as above.

Intestinal cells isolation and organoids culture

Intestinal stem cells were isolated from 12 weeks-old AKP and AKPP females 4 days after i.p. injection with 50mg/kg tamoxifen (Sigma), as previously described (1, 11). Briefly, ileum was flushed with ice-cold PBS supplemented with 2.5µg/ml Fungizone (Gibco) and 100µg/ml Normocin (InvivoGen) and the Peyer's patches were removed. The ileum was cut into 1.5cm pieces, incubated in 1mM EDTA in PBS at room temperature for 30 minutes and digested in DMEM (Gibco) with 2mM $CaCl_2$, 3mg/ml Collagenase IV (Worthington Biochemical C) and 100U DNaseI (Roche) for 20 minutes at 37°C. The single cell suspension was mixed with (Corning) at 3000 cells/disk ($2x10^{-5}$cells/ml) and plated into 24 well plates. Matrigel was allowed to polymerize for 15 minutes at 37°C and cells were cultured in advanced DMEM/F12 supplemented with B-27, N-2 and 50µg/ml gentamicin (Gibco). The colony number and the individual organoid diameter were quantified 1 week after plating, either automatically by converting the pictures into binary image and running a particle analysis with ImageJ (NIH), or manually by drawing the organoids surface area with ImageJ and QuPath (QuPath). For cell harvesting Matrigel was dissolved using Cell Recovery Solution (Corning) under rotation at 60rpm for 20 minutes at +4°C. For subsequent passaging, the organoids were dissociated in TrypLE Select (1x) (Gibco) for 5 minutes at 37°C, the cells were washed, counted and 1000 cells/ 50 µl of Matrigel were cultured again as above. For staining, the organoids were gently collected by centrifugation for 5 minutes at 600rpm, fixed for 10 minutes in 4%PFA, embedded into 2% agarose (Sigma) and processed for paraffin embedding and sectioning.

Fibroblast isolation

The ileums of 8-12 week old mTmG$^+$ (12) or wild type female mice were dissected, flushed with ice-cold PBS and Peyer's patches were removed. The intestine was cut into 1.5cm pieces, incubated in 15mM EDTA at 37°C for 20 minutes, and the epithelium was mechanically removed by vortexing. The mesenchymal fraction was minced into 2mm pieces and digested with Liberase TL (Roche) in DMEM with 2% FCS at 37°C for 45 minutes. The CD45$^+$ cells were depleted using mouse CD45 nanobeads (Biolegend). The remaining cells were cultured in DMEM with 1mM Glutamax, 10%FBS, 1%Hepes and Gentamycin 50µg/ml (Gibco) for 1 week. The tdTomato$^+$ or wild type fibroblast purity was confirmed by staining on coverslips for endothelial cells (rabbit anti-mouse CD31, Abcam), immune cells (rat anti-mouse CD45, BD), and fibroblasts markers (rat anti-mouse Podoplanin, MBL, and goat anti-mouse smooth muscle actin, Abcam). Fibroblasts from passages 2 or 3 were used for experiments.

Organoids *in vivo* implantation and tumor dissociation

For subcutaneous tumors, organoids were grown for 3 days in Matrigel, gently collected as described above, re-suspended in pure Advanced DMEM/F-12 with 50% 8mg/ml diluted Matrigel (Corning), and injected subcutaneously using 20G needle (Braun). For implantation of second generation organoids, 50 AKP and 300 AKPP parental organoids (1st) were injected in NSG mice and new organoids harvested from 400mm^3 large tumors (2nd), respectively on day 25 (AKP tumor derived, named F3A8) or day 41 (AKPP tumor derived, named F3P16). Tumors were minced into 2mm^3 pieces, incubated for 10 minutes in 5 mM EDTA at room temperature, digested for 30 minutes at 37°C in Trypsin10x (Gibco) supplemented with 100U DNaseI, filtered with 70µm strainer and passaged 3 times before re-implantation, as above.

To study the kinetics of the desmoplastic model, two different conditions were used. In one 50 AKP or AKPP organoids were implanted per mouse and tumors were excised when they reached at least 400mm^3, AKP on day 26 and AKPP on day 93. In second case 8 AKP or 50 AKPP were implanted per mouse in order to obtain slower AKP growth and tumors were collected when they become palpable, AKP day 40 and AKPP day 48 (Figure S2E).

For intestinal fibroblast co-implantation experiments because of slow growth of AKPP tumors 5000 tdTomato$^+$ fluorescent fibroblasts were co-injected with 50 AKP (100:1) or 300 AKPP (16:1) organoids per mouse (Figures 3I-L and S2H). The presence of tdTomato$^+$ cells in resected tumors was verified using fluorescence stereomicroscope (Leica M205 FA). In chemotherapy experiments, 50 AKP or dlNGFR-AKP and 300 AKPP (ratio 1:6) or 100 AKP-MMP14 (ratio 1:2) organoids in order to obtain comparable control growth curves (Figure 3 and Figure 4).

Organoids co-culture and treatment

For experiments in hydrogels, 500 AKP or AKPP cells in presence or absence of 1000 tdTomato$^+$ intestinal fibroblasts, were embedded in mechanically dynamic enzymatically crosslinked polyethylene glycol (PEG) hydrogels, with full-length fibronectin replaced by MMPs sensitive RGDs (Arg-Gly-Asp). The overall content of PEG was controlled resulting in dissimilar initial mechanical properties. The hydrogels soften in time thanks to ester-based hydrolysis, allowing both CSC expansion and organoids formation. The synthesis of hydrogel precursors and formation of dynamic PEG hydrogels, were described previously (13). The approximate initial stiffness tested was either 1.3kPa or 2.7kPa. Polymerization of hydrogels was allowed for 15 minutes at 37°C. Organoids were then cultured 5 days in 50% complete stem cell medium and 50% DMEM with 1mM Glutamax, 10%FBS, and 1%Hepes. Pictures of each well were captured with stereomicroscope (Leica M205 FA), and organoids number and diameter were quantified.

For studies of 5-FU and cisplatin effects on organoids *in vitro* 1000 AKP or AKPP cells were plated in 50µl Matrigel disks and cultured for 3 days in stem cell medium. The organoids were treated with 0, 0.1, 1, 10, 50 or 100µM 5-FU or cisplatin, and cultured for 3 more days. Pictures of the individual wells were acquired under stereomicroscope (Leica M205 FA). For *in vitro* organoid and fibroblast co-cultures, 1000 AKP or AKPP cells were embedded in 50µl Matrigel disks placed in a 12 transwell insert and cultured for 3 days in stem cell medium. $10x10^4$ intestinal fibroblasts were then plated in the corresponding well and the cells were co-cultured for 1.5 days in 50% stem cell medium and 50% DMEM with 1mM Glutamax, 10% FBS, and 1% Hepes. 1000 AKP or AKPP cells embedded in Matrigel disks, or $10x10^4$ intestinal fibroblasts in monolayer were also plated individually in 12 well dishes in 50% stem cells, 50% fibroblasts medium for 4 days and treated for 12 hours with either 2.5µM 5-FU or PBS. Fibroblasts were also treated with 50ng/ml mouse TGFß1 (fibroblast experiments only, Peprotech). Organoids and fibroblasts were harvested in RLT buffer and mRNA was isolated using Rneasy plus mini kit (Qiagen). Experiments were performed 3 times in duplicates.

Lentiviral vector (LV) production and CSC transduction.
We cloned the cDNA coding for *Anxa1* and *Mmp14* from mouse AKPP organoids. RNA was isolated using Rneasy Mini kit (Qiagen) and reverse transcribed using the SuperScript III (Vilo kit, Invitrogen). *Anxa1* and *Mmp14* were amplified using the PfuUltra II Fusion HS DNA polymerase (Agilent Technologies), according to the manufacturer's instructions, using the following primers: Anxa1: (BamHI) GAGTCTCTCTTCAGTCCCCG; (SalI) CCCATGCCATCGAAGGAAAAC; Mmp14: (BamHI) GAAGACAAAGGCGCCCCAA; (SalI) AGGGTGGGAGAGGCCAATTA. All primers incorporated a DNA sequence containing a modified BamHI (AAAAAGGATCC) or a SalI (AAAAAGTCGAC) restriction site as indicated. The resulting amplicons were cloned into BamHI and SalI restriction sites of a previously described LV plasmid (14) under the transcriptional control of the spleen focus-forming virus promoter. Vesicular stomatitis virus (VSV)-pseudotyped third-generation LVs were produced by transient transfection of 293T cells, concentrated and titered as previously described (14). $1x10^4$ AKP cells were transduced at MOI≥20. LVs expressing truncated non-functional low affinity nerve growth factor receptor were used as control. LVs were diluted in CSC growth medium with 10µM Y-27632 (StemCell Technologies). The cancer cells were added to the infection medium, spinoculated 1 hour at 600g and 32°C, incubated for 6 hours at 37°C, washed and embedded in 50µl Matrigel. The expression of *Anxa1* and *Mmp14* was confirmed by qPCR and staining (data not shown).

Real Time PCR
Tumor fragments were washed twice in ice-cold PBS and snap-frozen on dry ice. For RNA isolation tumors were submerged in QIAzol lysis reagent (Qiagen) and homogenized using Fast Prep-24 disruptor (MP). The RNA was extracted by bisphenol/chloroform/isoamyl-alcohol gradient (Biosolve) and further purified on Rneasy plus columns (Qiagen). *In vitro* cultured cells were lysed with RLT buffer and RNA was isolated using Rneasy plus columns (Qiagen). The RNA quality was verified using 2100 Bioanalyzer (Agilent). Reverse transcription first strand cDNA synthesis kit (Roche) was used to obtain cDNA, and real-time qPCR was performed using Sensi-Fast SYBR Lo-Rox Kit (Bioline), with 1µM primer pairs, on QuantStudio-3 (Applied Biosystem). Primers used are listed in Supplemental Table 2. Gene expression was analyzed by comparative Ct (ΔΔCt) method.

RT-qPCR results are shown as fold change over controls, either as scatter plots with mean±SD or heatmaps. Heatmaps were generated with pheatmap R package.

Immunoblotting

Organoids were retrieved with Cell Recovery Solution (Corning) and lysed in RIPA buffer, supplemented with protease and phosphatase inhibitors (Roche). Protein concentration was quantified using BCA (Pierce), 10µg protein were loaded with 1x Laemmli buffer on 10% Mini-PROTEAN TGX gels (Biorad), transferred on a PVDF membrane (Millipore), incubated overnight with primary antibodies for goat anti-human PROX1 (R&D Systems), rabbit anti-human Phospho-Histone3 (Cell Signaling) or rabbit anti-mouse Actin (Sigma), and detected by HRP-conjugated secondary antibodies (Dako) using by chemoluminescent substrate emission (Thermo Scientific) on a Fusion Fx Imaging System (Vilber).

Immunofluorescent and histological staining

Tumors were fixed in 4% PFA and embedded into paraffin. 5µm sections were deparaffinized, treated with Tris- or Citrate-Based antigen retrieval buffer (Vector laboratories), blocked with 5% donkey serum, 0.5%BSA and 0.3% TritonX100 solution in PBS, or with mouse IgG blocking reagent (Vector laboratories), incubated with primary antibodies and with donkey secondary antibodies conjugated to Alexa 488, 555 and 647 fluorophores (Invitrogen). The details of antibodies are provided in the Supplemental Table 4. Sections were mounted in Fluoromount-G mounting medium with DAPI (eBioscience). Alternatively, tumor sections were stained using Masson's trichrome procedure (Sigma) or with H&E using Harris modified hematoxylin and eosin solutions (Sigma) and slides were mounted in Aquatex (Merck). For whole-mount immunofluorescent staining, 4-8mm^3 tumor pieces were fixed in 4% PFA for 12 hours, equilibrated in 30% sucrose for 48 hours, embedded in 4% agarose and cut into 200µm slices with a microtome. Slices were incubated in 24 well plates with blocking solution for 6-8 hours, overnight with either primary or secondary antibodies, and cleared for minimum 36 hours at 70 rpm and +4°C in 1.62 M Histodenz (Sigma) and 0.1% Tween20 (Sigma) in PBS.

FACS analysis

400mm^3 of tumor, 200mm^3 of spleen and entire mesenteric lymph node from each mouse were collected in ice cold MACS buffer with 4% FBS, 2mM EDTA (Sigma) and 50µg/ml gentamicin (Gibco) in PBS. One half of tumor sample was mechanically dissociated by scissors and washed in ice cold PBS; the second half was digested in an IMDM solution (Sigma) with 1mg/ml Collagenase/Dispase (Roche) and 20µg/ml DNaseI (Roche) with shaking at 330rpm for 20 minutes at 37°C. The lymph node was minced with scissors and digested as above. The spleen was mechanically dissociated and treated with red blood cells 1x RBC Lysis Buffer (Invitrogen) for 5 minutes on ice. Samples were filtered through 40µm strainer and stained with conjugated primary antibodies in presence of Fc block. Antibodies and the corresponding dilutions are listed in Supplemental Table 3. Before analysis, the cells were re-suspended in DAPI-containing MACS solution (Sigma). For intracellular staining, the cells were incubated for 20 minutes in Zombie Violet (Biolegend) diluted in ice cold PBS, stained for membrane receptors, fixed with Cytofix/Cytoperm (BD) for 20 minutes, stained for intracellular proteins and resuspended in Perm/Wash solution 1x (BD). For acquisition, an LSRII flow cytomer (BD) was used. A common acquisition matrix was automatically generated for all panels simultaneously, based on single stained setup beads (BD) and compensations were adjusted during analysis, based on fluorescence minus one (FMO) controls, prepared as a mixture of several samples, specific to each panel. The analysis was performed with FlowJo version 9 (FlowJo LLC). Data are presented as percentage of total CD45$^+$ viable population, unless specified otherwise. Gating strategies for tumor, spleen and mesenteric lymph node are presented in Supplemental Figure 7J-L.

Mouse tumor RNA-seq

RNA QC, library preparations, and sequencing reactions were conducted at GENEWIZ, LLC. (South Plainfield, NJ, USA). Total RNA samples were quantified using Qubit 2.0 Fluorometer (Life Technologies, Carlsbad, CA, USA) and RNA integrity was checked with 4200 TapeStation (Agilent Technologies, Palo Alto, CA, USA). RNA sequencing library preparation used NEBNext Ultra RNA Library Prep Kit for Illumina by following the manufacturer's recommendations (NEB, Ipswich, MA, USA). Briefly, enriched RNAs were fragmented for 15 minutes at 94 °C. First strand and second strand cDNA were subsequently synthesized. cDNA fragments were end-repaired and adenylated at 3'ends, and universal adapter was ligated to cDNA fragments, followed by index addition and library enrichment with limited cycle PCR. Sequencing libraries were validated on the Agilent TapeStation (Agilent Technologies, Palo Alto, CA, USA), and quantified by using Qubit 2.0 Fluorometer (Invitrogen, Carlsbad, CA) as well as by quantitative PCR (Applied Biosystems, Carlsbad, CA, USA). The sequencing libraries were clustered on two lanes of a flowcell. After clustering, the flowcell was loaded on the Illumina HiSeq instrument according to manufacturer's instructions. The samples were sequenced using a 2x150 Paired End (PE) configuration. Image analysis and base calling were conducted by the HiSeq Control Software (HCS). Raw sequence data (.bcl files) generated from Illumina HiSeq was converted into fastq files and de-multiplexed using Illumina's bcl2fastq 2.17 software. One mismatch was allowed for index sequence identification.

Image acquisition and quantifications

For histological analyses, three or more representative pictures per tumor were taken using LSM 880 with Airyscan confocal microscope (Zeiss, 20x or 40x objective). Alternatively, the entire tumor area was acquired using an AxioScan.Z1 fluorescence scanner (Zeiss, 20x objective) on a 2 layers Z-stack. For the analyses of AP, APP, AKP and AKPP tumors and their responses to chemotherapy at least three pictures per tumor were taken and used for the quantification. For all other quantifications, the entire tumor area was analysed. Quantifications were performed with ImageJ (NIH) by encoding macros in RGB batch mode, where a threshold was fixed for each channel, and the percentage of positive over total area was used as output. All stainings performed are listed in Supplemental Table 4, while all exceptions in data analysis are listed below. In staining for PH3, α-SMA and E-cadherin, the number of proliferating cells was quantified using particle analysis (size 50-infinity). The proliferation of stromal (α-Sma$^+$) and cancer cell (E-cadherin$^+$) compartments was measured as the overlap of PH3 with each area selection, upon =3 pixels mask enlargement. Tumor cell death was manually marked in QuPath (cell counter), and calculated as the percentage of necrotic tumor glands over the total number. Stainings for α-Sma, PROX1 and for Ki67 and E-cadherin, PROX1 and Ki67 were also analysed in the same way. In staining for CD8a, VE-cadherin and E-cadherin, the number and area of vessels as well as the number of CD8$^+$ T cells were quantified by particle analysis (respectively size 60-infinity and 50-infinity). The mask of CD8a$^+$ cells was memorized and the quantity of infiltrated cells into tumor area was calculated by the overlap with the E-cadherin$^+$ signal (select, set background to 0, clear outside). The CD8a$^+$ intraepithelial infiltration and number of tumor glands infiltrated by CD8a$^+$ T cells, as well as the VE-cadherin$^+$ vessel number and size, were also verified manually, with cell counter and drawing areas in QuPath. In staining for CD31, α-Sma and E-cadherin, number and caliber of vessels were summarized by particle analysis (size 60-infinity), the CD31 mask was enlarged of =2 pixel, and the mural cell coverage was measured as the overlap of α-Sma$^+$ signal in the vascular selection. The same analysis was performed for VE-Cadherin, α-Sma and E-cadherin stainings. In staining for FOXP3, CD4 and E-cadherin, the number of CD4$^+$ T cells were calculated by particle analysis (50-infinity), the mask was memorized and the percentage of Tregs was calculated as the overlap with FoxP3 signal. The same approach was also used for CD8a, GrzB and E-cadherin. In staining for CD44v6, PROX1 C-term and β-Catenin, PROX1 overlap was measured within the selection of CD44V6 mask upon pixels =3 enlargement. In staining for actin, Krt20 and E-cadherin the differentiation was measured as the overlap of Krt20 signal over the E-cadherin selection. In staining for phosphoStat3, α-Sma and CD44, the phosphoStat3 signal was evaluated both inside and in the inverted (make inverse, clear outside) α-Sma^+ selection, upon mask pixles=3 enlargement. In staining for α-Sma, PROX1 and MMP14, the software was also instructed to memorize the α-Sma^+ area (create selection and add in ROI manager) and to measure the co-localization (overlap) with MMP14. In stainings for γH2AX, α-Sma, and E-cadherin, as γH2AX staining occurs in several patterns, the analysis was done on representative pictures taken with LSM 880 confocal microscope (Zeiss). The DNA damage response was analyzed manually with cell counter on QuPath, tagging the α-Sma^+ or E-$cadherin^+$ cells positive for $\gamma H2AX^+$ nuclear foci. Dead cells with diffuse γH2AX staining were excluded. In stainings for B220, α-Sma and E-cadherin, the number of $B220^+$ B cells was quantified by particle analysis (50-infinity). For quantification of tertiary lymphoid structures, the ROI containing clusters of minimum 10 B220+ B cells were quantified and measured. For liver analysis in T cell-depletion experiment sections from one lobe from each liver was stained for VE-cadherin, α-Sma and Cdx2. The total fibrosis area is presented; $Cdx2^+$ cancer cells were not quantified as only few micrometastases were found.

Mouse tumor RNA-seq data analyses

RNA-seq quantification was performed using kallisto (15). In brief, target transcript sequences were obtained from ENSEMBLE (GRCm38.p6), and the abundance of transcripts were quantified using kallisto 0.44.0 with sequence-based bias correction. All other parameters were set to default when running kallisto. Kallisto's transcript-level estimates were further summarized at the gene-level using tximport 1.8.0 from Bioconductor (16). Both raw data and gene-by-sample matrix of estimated counts are publicly accessible via GSE124716. For downstream analysis, lowly abundant genes were filtered out and unwanted variation was estimated using the RUVr functionality from the RUVseq 1.16.0 package within Bioconductor (17). The number of factors of unwanted variation to be estimated from the data was set to 4, and the genes-by-samples matrix of residuals was obtained from a first-pass quasi-likelihood negative binomial generalized log-linear regression of the counts on the biological covariates using the edgeR package from Bioconductor (18). Differential expression analysis was performed using DESeq2 1.22.0 from Bioconductor (19), with estimated factors of unwanted variation included as additional covariates in the design formula. Significant genes were identified using FDR<0.05 and fold change>2 for APP *vs.* AP comparison, and FDR<0.05 and fold change>1.5 for treated *vs.* untreated comparison. Gene Set Enrichment Analysis (GSEA) was performed using fgsea 1.8.0 package from Bioconductor (preprint from Sergushichev 2016, bioRxiv) with log2foldchange values returned by DESeq2 as gene-level statistic. Prior to GSEA, mouse genes were converted to human orthologs using biomaRt 2.38.0 from Bioconductor (20). If a human ortholog was associated with more than one mouse gene, the mouse gene with maximum mean expression was selected using the collapseRows functionality within the WGCNA R package (21). Signaling pathways analyzed by GSEA were obtained from the Hallmark gene sets of the MSigDB (22). Gene signatures of murine hematopoietic cells were obtained from Haemopedia database (23). RNA-seq data are deposited in Gene Expression Omnibus under the accession number GSE124716.

Analyses of publicly available human CRC data.

Processed gene expression and metadata of human CRC tumors as previously reported in (24) were obtained from Gene Expression Omnibus under GSE39582. Additional metadata including MSI status and CMS classification labels for this data set were obtained from the Colorectal Cancer Subtyping Consortium (CRCSC, (25). CRC intrinsic subtypes (CRIS) classification labels were separately obtained from (26). Of the 566 tumor samples available, 75 samples were classified as MSI and thus were excluded; leading to 444 MSS CRC samples for downstream analyses. Probe annotation data were obtained from GSE39582, and normalized intensity values were summarized at the gene level using the collapseRows functionality within the WGCNA R package (21), with the collapsing method set to MaxMean. Tumors were stratified as PROX1-high or PROX1-low using median expression of PROX1, and the association with survival was assessed using log-rank test from survival R package Enrichment of Hallmark gene sets of the MSigDB (22) was assessed using single-sample GSEA (ssGSEA) method of (27), as implemented in the GSVA Bioconductor package (28). Human stromal gene signature was obtained from (29), and similarly assessed with ssGSEA. To assess the enrichment of mouse APP vs. AP gene signature in human CRC tumors, first the list of significant genes derived from the RNA-seq data was converted to human orthologs using biomaRt 2.38.0 from Bioconductor (20). Next, for genes belonging to the signature, expression data was z-score transformed per gene across the samples. Finally, an enrichment score was computed per sample as sum of the z-scores for down-regulated genes subtracted from the sum of z-scores for up-regulated genes. Intuitively, the higher the similarity of the expression pattern in human CRC tumors to the APP *vs*. AP signature, the greater will be the enrichment score.

Supplemental References

1. Ragusa S, Cheng J, Ivanov KI, Zangger N, Ceteci F, Bernier-Latmani J, et al. PROX1 promotes metabolic adaptation and fuels outgrowth of Wnt(high) metastatic colon cancer cells. *Cell Rep.* 2014;8(6):1957-73.
2. Shibata H, Toyama K, Shioya H, Ito M, Hirota M, Hasegawa S, et al. Rapid colorectal adenoma formation initiated by conditional targeting of the Apc gene. *Science.* 1997;278(5335):120-3.
3. el Marjou F, Janssen KP, Chang BH, Li M, Hindie V, Chan L, et al. Tissue-specific and inducible Cre-mediated recombination in the gut epithelium. *Genesis.* 2004;39(3):186-93.
4. Marino S, Vooijs M, van Der Gulden H, Jonkers J, and Berns A. Induction of medulloblastomas in p53-null mutant mice by somatic inactivation of Rb in the external granular layer cells of the cerebellum. *Genes Dev.* 2000;14(8):994-1004.
5. Lavado A, Lagutin OV, Chow LM, Baker SJ, and Oliver G. Prox1 is required for granule cell maturation and intermediate progenitor maintenance during brain neurogenesis. *PLoS Biol.* 2010;8(8).
6. Risebro CA, Searles RG, Melville AA, Ehler E, Jina N, Shah S, et al. Prox1 maintains muscle structure and growth in the developing heart. *Development.* 2009;136(3):495-505.
7. Johnson NC, Dillard ME, Baluk P, McDonald DM, Harvey NL, Frase SL, et al. Lymphatic endothelial cell identity is reversible and its maintenance requires Prox1 activity. *Genes Dev.* 2008;22(23):3282-91.
8. Petrova TV, Makinen T, Makela TP, Saarela J, Virtanen I, Ferrell RE, et al. Lymphatic endothelial reprogramming of vascular endothelial cells by the Prox-1 homeobox transcription factor. *EMBO J.* 2002;21(17):4593-9.
9. Seth A, Ye J, Yu N, Guez F, Bedford DC, Neale GA, et al. Prox1 ablation in hepatic progenitors causes defective hepatocyte specification and increases biliary cell commitment. *Development.* 2014;141(3):538-47.
10. Cespedes MV, Espina C, Garcia-Cabezas MA, Trias M, Boluda A, Gomez del Pulgar MT, et al. Orthotopic microinjection of human colon cancer cells in nude mice induces tumor foci in all clinically relevant metastatic sites. *Am J Pathol.* 2007;170(3):1077-85.
11. Sato T, Stange DE, Ferrante M, Vries RG, Van Es JH, Van den Brink S, et al. Long-term expansion of epithelial organoids from human colon, adenoma, adenocarcinoma, and Barrett's epithelium. *Gastroenterology.* 2011;141(5):1762-72.
12. Muzumdar MD, Tasic B, Miyamichi K, Li L, and Luo L. A global double-fluorescent Cre reporter mouse. *Genesis.* 2007;45(9):593-605.
13. Gjorevski N, Sachs N, Manfrin A, Giger S, Bragina ME, Ordóñez-Morán P, et al. Designer matrices for intestinal stem cell and organoid culture. *Nature.* 2016;539:560.
14. Squadrito ML, Cianciaruso C, Hansen SK, and De Palma M. EVIR: chimeric receptors that enhance dendritic cell cross-dressing with tumor antigens. *Nat Methods.* 2018;15(3):183-6.
15. Bray NL, Pimentel H, Melsted P, and Pachter L. Near-optimal probabilistic RNA-seq quantification. *Nat Biotechnol.* 2016;34(5):525-7.
16. Soneson C, Love MI, and Robinson MD. Differential analyses for RNA-seq: transcript-level estimates improve gene-level inferences. *F1000Res.* 2015;4:1521.
17. Risso D, Ngai J, Speed TP, and Dudoit S. Normalization of RNA-seq data using factor analysis of control genes or samples. *Nat Biotechnol.* 2014;32(9):896-902.
18. Robinson MD, McCarthy DJ, and Smyth GK. edgeR: a Bioconductor package for differential expression analysis of digital gene expression data. *Bioinformatics.* 2010;26(1):139-40.
19. Love MI, Huber W, and Anders S. Moderated estimation of fold change and dispersion for RNA-seq data with DESeq2. *Genome Biol.* 2014;15(12):550.

20. Durinck S, Spellman PT, Birney E, and Huber W. Mapping identifiers for the integration of genomic datasets with the R/Bioconductor package biomaRt. *Nat Protoc.* 2009;4(8):1184-91.
21. Miller JA, Cai C, Langfelder P, Geschwind DH, Kurian SM, Salomon DR, et al. Strategies for aggregating gene expression data: the collapseRows R function. *BMC Bioinformatics.* 2011;12:322.
22. Liberzon A, Birger C, Thorvaldsdottir H, Ghandi M, Mesirov JP, and Tamayo P. The Molecular Signatures Database (MSigDB) hallmark gene set collection. *Cell Syst.* 2015;1(6):417-25.
23. de Graaf CA, Choi J, Baldwin TM, Bolden JE, Fairfax KA, Robinson AJ, et al. Haemopedia: An Expression Atlas of Murine Hematopoietic Cells. *Stem Cell Reports.* 2016;7(3):571-82.
24. Marisa L, de Reynies A, Duval A, Selves J, Gaub MP, Vescovo L, et al. Gene expression classification of colon cancer into molecular subtypes: characterization, validation, and prognostic value. *PLoS Med.* 2013;10(5):e1001453.
25. Guinney J, Dienstmann R, Wang X, de Reynies A, Schlicker A, Soneson C, et al. The consensus molecular subtypes of colorectal cancer. *Nat Med.* 2015;21(11):1350-6.
26. Isella C, Brundu F, Bellomo SE, Galimi F, Zanella E, Porporato R, et al. Selective analysis of cancer-cell intrinsic transcriptional traits defines novel clinically relevant subtypes of colorectal cancer. *Nat Commun.* 2017;8:15107.
27. Barbie DA, Tamayo P, Boehm JS, Kim SY, Moody SE, Dunn IF, et al. Systematic RNA interference reveals that oncogenic KRAS-driven cancers require TBK1. *Nature.* 2009;462(7269):108-12.
28. Hanzelmann S, Castelo R, and Guinney J. GSVA: gene set variation analysis for microarray and RNA-seq data. *BMC Bioinformatics.* 2013;14:7.
29. Yoshihara K, Shahmoradgoli M, Martinez E, Vegesna R, Kim H, Torres-Garcia W, et al. Inferring tumour purity and stromal and immune cell admixture from expression data. *Nat Commun.* 2013;4:2612.

Supplemental Tables

Supplemental Table 1, related to Figure 1.
PROX1 and stromal abundance scores in 114 MSS primary CRC.

Histopathology score in human CRC samples				Histopathology score in human CRC samples				Histopathology score in human CRC samples			
Tumor_ID	PROX1 Score	Stroma Score	Sex	Tumor_ID	PROX1 Score	Stroma Score	Sex	Tumor_ID	PROX1 Score	Stroma Score	Sex
1	2	2	NA	39	2	2	NA	77	2	3	NA
2	1	2	NA	40	3	1	NA	78	2	2	NA
3	1	2	NA	41	0	3	NA	79	1	2	NA
4	2	2	NA	42	2	2	NA	80	1	2	NA
5	1	3	NA	43	0	3	NA	81	3	1	NA
6	1	2	NA	44	3	2	NA	82	2	3	NA
7	0	3	NA	45	2	2	NA	83	1	2	NA
8	2	2	NA	46	1	2	NA	84	4	1	NA
9	4	1	NA	47	1	1	NA	85	2	1	NA
10	1	3	NA	48	1	4	NA	86	1	2	NA
11	2	2	NA	49	2	1	NA	87	3	1	NA
12	3	3	NA	50	2	2	NA	88	4	1	NA
13	2	1	NA	51	1	2	NA	89	2	2	NA
14	4	2	NA	52	1	2	NA	90	1	2	NA
15	0	2	NA	53	1	4	NA	91	1	1	NA
16	2	2	NA	54	1	3	NA	92	4	1	NA
17	1	2	NA	55	1	2	NA	93	1	2	NA
18	1	2	NA	56	1	2	NA	94	1	3	NA
19	0	3	NA	57	1	2	NA	95	0	2	NA
20	1	2	NA	58	2	1	NA	96	1	3	NA
21	1	2	NA	59	2	4	NA	97	1	1	NA
22	1	2	NA	60	1	2	NA	98	1	1	NA
23	2	1	NA	61	0	2	NA	99	1	2	NA
24	1	2	NA	62	2	2	NA	100	1	2	NA
25	1	1	NA	63	2	1	NA	101	2	2	NA
26	3	2	NA	64	1	2	NA	102	1	3	NA
27	2	2	NA	65	2	2	NA	103	2	1	NA
28	1	4	NA	66	1	3	NA	104	0	3	NA
29	2	2	NA	67	2	3	NA	105	1	2	NA
30	1	2	NA	68	1	3	NA	106	0	3	NA
31	1	1	NA	69	2	2	NA	107	1	2	NA
32	2	2	NA	70	1	2	NA	108	0	3	NA
33	2	1	NA	71	4	1	NA	109	1	2	NA
34	3	2	NA	72	1	1	NA	110	0	4	NA
35	3	2	NA	73	1	3	NA	111	2	3	NA
36	2	3	NA	74	2	2	NA	112	1	1	NA
37	0	3	NA	75	3	1	NA	113	1	2	NA
38	1	4	NA	76	0	3	NA	114	0	3	NA

Supplemental Table 2, related to Figure 2-7. Sequences of primers.

Gene Symbol	Fwd seq.	Rev Seq.	Source
Prox1	GCAGGCCTACTATGAGCCAG	TGATATTCTCAACCCGGGCG	https://doi.org/10.1016/j.celrep.2014.08.041
Lgr5	CCTACTCGAAGACTTACCCAGT	GCATTGGGGTGAATGATAGCA	https://doi.org/10.1016/j.celrep.2014.08.041
Lef1	CTCGTCGCTGTAGGTGATGA	AAATGGGTCCCTTTCTCCAC	This paper
Rnf43	TCCGAAAGATCAGCAGAACAGA	GGACTGCATTAGCTTCCCTTC	https://doi.org/10.1016/j.celrep.2014.08.041
Ephb2	GCGGCTACGACGAGAACAT	GGCTAAGTCAAAATCAGCCTCA	https://doi.org/10.1016/j.celrep.2014.08.041
Cd44v6	CCTTGGCCACCACTCCTAATAG	CAGTTGTCCCTTCTGTCACATG	doi: 10.1074/jbc.M116.752451
Krt20	AGTTTTCACCGAAGTCTGAGT	GTAGCTCATTACGGCTTTGGAG	Primer Bank 21592285a1
Ki67	ATCATTGACCGCTCCTTTAGGT	GCTCGCCTTGATGGTTCCT	Primer Bank 1177528a1
Ccnb1	CTTGCAGTGAGTGACGTAGAC	CCAGTTGTCGGAGATAAGCATAG	Primer Bank 118130025c2
Fap	GTCACCTGATCGGCAATTTGT	CCCCATTCTGAAGGTCGTAGAT	Primer Bank 118131069c1
Postn	TGGTATCAAGGTGCTATCTGCG	AATGCCCAGCGTGCCATAA	Primer Bank 311771598c1
Pai1	CTGGGTGGAAAGGCATACCAAAG	TCCATTGGCCACTGAAGTAGAGG	This paper
Acta2	GTCCCAGACATCAGGGAGTAA	TCGGATACTTCAGCGTCAGGA	Primer Bank 6671507a1
Ctgf	GGGCCTCTTCTGCGATTTC	ATCCAGGCAAGTGCATTGGTA	Primer Bank 6753878a1
mCol6a1	CTGCTGCTACAAGCCTGCT	CCCCATAAGGTTTCAGCCTCA	Primer Bank 6753484a1
Cd31	AACAGAAACCCGTGGAGATG	GTCTCTGTGGCTCTCGTTCC	doi: 10.1242/dev.050021
Cdh5	CCCACGAAGTCCCTGGACTATG	GGTCTGTGGCCTCAATGTAGAATG	this paper
Kdr	CCCCAAATTCCATTATGACAACACAGC	CCGGCTCTTTCGCTTACTGTTC	this paper
Pdgfc	GCCAAAGAACGGGGACTCG	AGTGACAACTCTCTCATGCCG	PrimerBank 10242385a1
Sppn	AGCAAGAAACTCTTCCAAGCAA	GTGAGATTCGTCAGATTCATCCG	PrimerBank 6678113a1

Hbegf	CGGGGAGTGCAGATACCTG	TTCTCCACTGGTAGAGTCAGC	PrimerBank 6754178a1
Il1b	CAACCAACAAGTGATATTCTCCATG	GATCCACACTCTCCAGCTGCA	this paper
Il6	TAGTCCTTCCTACCCCAATTTCC	TTGGTCCTTAGCCACTCCTTC	PrimerBank 13624311a1
Vegfa	GCAAGAAATCCCGGTTTAAATCCTGG	GAGTCTGTGTTTTTGCAGGAACATTTAC	this paper
Mmp2	CAAGTTCCCCGGCGATGTC	TTCTGGTCAAGGTCACCTGTC	Primer Bank 6678902a1
Mmp14	CAGTATGGCTACCTACCTCCAG	GCCTTGCCTGTCACTTGTAAA	PrimerBank 31982191a1
Anxa1	ATGTATCCTCGGATGTTGCTGC	TGAGCATTGGTCCTCTTGGTA	Primer Bank 6754570a1
Ly6g	GAGGAAGTTTTATCTGTGCAGCC	TCAGGTGGGACCCCAATACA	This paper
Prf1	AGAGCATCCCTGACTTTCCC	ATGTTTACGCTTCGTGGCAG	This paper
Gzma	AGACACGGTTGTTCCTCACTC	ATCAAAGCGCCAGCACAGAT	This paper

Supplemental Table 3, related to Figure 6 and 7.
Staining conditions for flow cytometry.

Antigen	Conjugate	Clone	Concentration	Provider	Dilution
CD11b	Briliant Violet 711	M1/70	50µg/ml	BioLegend	1:200
CD11c	PE-Cy7	N418	0.2mg/ml	BioLegend	1:200
CD3	Briliant Violet 605	17A2	100µg/ml	BioLegend	1:50
CD4	Brillant Violet 785	RM4-5	50µg/ml	BioLegend	1:100
CD44	Alexa Fluor 488	IM7	0.5mg/ml	BioLegend	1:200
CD45	APC	30-F11	0.2mg/ml	eBioscience	1:100
CD45	APC-eFluor 780	30-F11	0.2mg/ml	eBioscience	1:200
CD45R	Brillant Violet 605	RA3-6B2	100µg/ml	BioLegend	1:200
CD62L	PE-Cy7	MEL-14	0.2mg/ml	BioLegend	1:200
CD86	APC-Cy7	GL-1	0.2mg/ml	BioLegend	1:100
CD8a	R-PE	5H10	0.1mg/ml	Invitrogen	1:200
CD8a	PE-Cy7	5H10	0.1mg/ml	Life Technologies	1:200
F4/80	Alexa Fluor 488	BM8	0.5mg/ml	BioLegend	1.100
Fc block	Unconjugated	2.4G2	0.5mg/ml	BD Biosciences	1.100
FOXP3	Alexa Fluor 647	150D	100µg/ml	BioLegend	1:100
Granzyme B	FITC	GB11	100µg/ml	BioLegend	1:100
IFN-γ	PE	XMG1.2	0.2mg/ml	BD Biosciences	1:300
Ly6G	Brilliant Violet 605	1A8	0.2mg/ml	BioLegend	1:200
MHC class II	PerCP-Cy5.5	M5/114.15.2	0.2mg/ml	BioLegend	1:300

Supplemental Table 4, related to Figure 1-7. Antibodies and immunostaining conditions.

Antigen	Catalogue n°	Provider	Dilution	Retrieval
Phospho-Histone3	3377	Cell Signaling	1/300	High pH
Actin α-Smooth Muscle-Cy3	C6198	Sigma	1/200	
E-cadherin	AF748	R&D	1/200	
CD8a	14-0195-82	eBioscience	1/100	High pH
VE-cadherin	AF1002	R&D	1/200	
E-cadherin	3195S	Cell Signaling	1/200	
Prox1	AF2727	R&D	1/200	High pH
E-cadherin	3195S	Cell Signaling	1/200	
Ki67	556003	BD	1/200	
Periostin	AF2955	R&D	1/200	High pH
CD44v6	MCA1967	Biorad	1/200	
Actin α-Smooth Muscle-Cy3	C6198	Sigma	1/200	
PROX1	11-002	Angiobio	1/100	High pH
Smooth Muscle Actin	ab21027	Abcam	1/200	
Ki67	556003	BD	1/200	
CD31	ab28364	Abcam	1/100	Low pH
Actin α-Smooth Muscle-Cy3	C6198	Sigma	1/200	
E-cadherin	AF748	R&D	1/200	
VE-Cadherin	AF1002	R&D	1/200	High pH
Actin α-Smooth Muscle-Cy3	C6198	Sigma	1/200	
E-cadherin	3195S	Cell Signaling	1/200	
FoxP3	14-5773-80	eBioscience	1/100	High pH
CD4	ab183685	Abcam	1/200	
E-cadherin	AF748	R&D	1/200	
CD44v6	MCA1967	Biorad	1/200	Low pH
PROX1 C-term	OAAB15651	Lubio science	1/100	
β-Catenin	610154	BD	1/200	
Actin	A2066	Sigma	1/300	High pH
Cytokeratin 20	M0630	Dako	1/200	
E-cadherin	AF748	R&D	1/200	
PROX1	AF2727	R&D	1/100	High pH
Actin α-Smooth Muscle-Cy3	C6198	Sigma	1/200	
Desmin	ab15200	Abcam	1/300	
PROX1	AF2727	R&D	1/100	High pH
Fibronectin ab2033		Millipore	1/300	
Tenascin C	MAB2138	R&D	1/300	
Phospho-Stat3	9145	Cell Signaling	1/200	High pH
Smooth Muscle Actin	ab21027	Abcam	1/200	
CD44	550538	BD	1/200	
MMP14	ab51074	Abcam	1/200	High pH
Actin α-Smooth Muscle-Cy3	C6198	Sigma	1/200	
PROX1	AF2727	R&D	1/100	

Periostin	AF2955	R&D	1/200	High pH
Actin α-Smooth Muscle-Cy3	C6198	Sigma	1/200	
TenascinC	MAB2138	R&D	1/300	
phospho Histone H2AX	2577S	Cell Signaling	1/300	High pH
Actin α-Smooth Muscle-Cy3	C6198	Sigma	1/200	
E-cadherin	AF748	R&D	1/200	
CD8a	14-0195-82	eBioscience	1/100	High pH
GranzymeB	NB100-68455	Novus Biologicals	1/100	
E-cadherin	AF748	R&D	1/200	
B220/CD45R	14-0452-82	eBioscience	1/100	High pH
Actin α-Smooth Muscle-Cy3	C6198	Sigma	1/200	
E-cadherin	AF748	R&D	1/200	
B220/CD45R	14-0452-82	eBioscience	1/100	High pH
CD4	ab183685	Abcam	1/200	
VE-Cadherin	AF1002	R&D	1/200	
VE-Cadherin	AF1002	R&D	1/200	High pH
Actin α-Smooth Muscle-Cy3	C6198	Sigma	1/200	
CDX2	ab76541	Abcam	1/100	
CD8a	14-0195-82	eBioscience	1/100	High pH
CD4	ab183685	Abcam	1/200	
E-cadherin	AF748	R&D	1/200	
CD40	PA5-78980	Invitrogen	1/500	High pH
B220/CD45R	14-0452-82	eBiosciences	1/100	
Hypoxia	HP1-100	Natural Pharmacia International	1/100	Low pH